



Cite this: *J. Anal. At. Spectrom.*, 2023, **38**, 142

# High-precision double-spike Sn isotope analysis of geological materials by MC-ICP-MS†

Jia-Xin She, <sup>ab</sup> Weiqiang Li, <sup>\*ab</sup> Shichao An<sup>ab</sup> and Yuanfeng Cai<sup>a</sup>

Stable Sn isotopes have the potential to constrain the behavior of Sn in various natural and anthropogenic processes, however, studies on stable isotopes of Sn for terrestrial rock samples have been limited. Here, we present a high-precision Sn isotope analytical method of geological samples by the double spike technique. Samples were equilibrated with a  $^{117}\text{Sn}$ – $^{122}\text{Sn}$  double spike during dissolution, then Sn was purified from the rock matrix using TRU spec resin. The purified Sn solutions were analyzed on a Nu 1700 Sapphire MC-ICP-MS, and data reduction was performed using Newton–Raphson iteration. Effects of acid mismatch, concentration mismatch, and matrix elements were systematically tested to evaluate their impact on the accuracy and repeatability of the measurements. We show that the mismatch of acidity exerts negligible influences on the Sn isotope analysis. By contrast, the accuracy of Sn isotopic measurements could be compromised if the Sn concentration of the sample is below 40% of that of the standard. To ensure the accuracy of Sn isotope analysis, the concentration match between the sample and standard should be better than  $\pm 20\%$ . When the measured solution has varying mass ratios of  $[\text{X}]/\text{Sn}$  ( $\text{ng g}^{-1}/\text{ng g}^{-1}$ ) lower than 0.5 for Mg, Ca, Fe, Ti, U, Ni, Ag, As, Ru, and Mo, the measured Sn isotope composition was not affected. However, Cd in Sn samples could affect the accuracy of Sn isotope analysis by the  $^{117}\text{Sn}$ – $^{122}\text{Sn}$  double spike through the generation of  $^{116}\text{CdH}^+$  in plasma that interferes with  $^{117}\text{Sn}^+$ . The Cd/Sn ratio needs to be below 0.01 to ensure analytical accuracy by the double spike method. The accuracy of this method was further verified by measuring the pure solution with both double spike and sample standard bracketing methods, as well as processing a synthetic solution through column chemistry. The Sn isotope compositions of geological samples measured using our method are reproducible and consistent with previous data from other laboratories. Additionally, Sn isotope data for geological reference materials BIR-1, RGM-1, and GSR-1 are reported for the first time. Based on repeated analyses of pure and geological reference materials, the long-term intermediate precision is better than  $\pm 0.069\%$  on  $\delta^{122/118}\text{Sn}$  for a spiked solution of  $100 \mu\text{g g}^{-1}$ .

Received 18th October 2022  
Accepted 16th November 2022

DOI: 10.1039/d2ja00339b

rsc.li/jaas

## 1. Introduction

Tin (Sn) plays an important role in various geological and cosmochemical processes due to its lithophile, moderately siderophile, chalcophile, and moderately incompatible geochemical properties.<sup>1–4</sup> Tin is a major component of bronze and is important in archeological studies. Tin is a redox-sensitive element with mainly two oxidation states,  $\text{Sn}^{2+}$  and  $\text{Sn}^{4+}$ , both of which play important roles in petrogenesis and ore-forming processes.<sup>5–11</sup> Tin could complex with various ligands and exist in various geological materials<sup>2,12–18</sup> and could be enriched during chemical weathering and the Earth

differentiation processes to form granite-related Sn mineralization.<sup>19–22</sup> Natural Sn abundance is  $0.17 \mu\text{g g}^{-1}$  in the mantle and  $1.7 \mu\text{g g}^{-1}$  in the crust,<sup>23,24</sup> while it reaches a weight-percent level in Sn ores. Due to the “magic number” closed proton shell in its nucleus,<sup>25</sup> Sn has ten stable isotopes with the largest mass variations in the periodic table.<sup>26–28</sup>

Stable Sn isotopes are a powerful tool for studying the behavior of Sn in various processes,<sup>5,8,9,29–31</sup> as well as tracking the provenance of Sn in various natural samples and archaeological artifacts,<sup>32–35</sup> thus there has been a long interest in the Sn isotope variability of natural and artificial Sn-bearing samples. Early studies used thermal ionization mass spectrometry (TIMS) for Sn isotope measurements,<sup>36–38</sup> however, the high ionization potential (7.3 eV) of Sn prevents efficient and stable ionization of Sn.<sup>1,25,36,37,39</sup> As a result, the analytical precision was limited to a level of  $0.12\text{--}0.17\%$ /amu for Sn isotopes by TIMS, hindering the studies of Sn isotope fractionation induced by magmatic and ore-forming processes.<sup>25,37,38</sup> In the recent decade, the applications of multi-collector inductively coupled plasma mass

<sup>a</sup>State Key Laboratory for Mineral Deposits Research, School of Earth Sciences and Engineering, Nanjing University, Nanjing, Jiangsu 210023, China. E-mail: liweiqiang@nju.edu.cn

<sup>b</sup>Frontiers Science Center for Critical Earth Material Cycling, Nanjing University, Nanjing, China

† Electronic supplementary information (ESI) available. See DOI: <https://doi.org/10.1039/d2ja00339b>

spectrometry (MC-ICP-MS) made precise Sn isotope measurement possible.<sup>32,39,40</sup> Different chemical purification procedures and mass spectrometric methods have been reported, and a boom of Sn isotope studies is ongoing.<sup>41–44</sup>

Presently, the majority of reported Sn isotopic data in the literature are from Sn-rich minerals such as cassiterite<sup>9,45–47</sup> or Sn-bearing materials such as bronze.<sup>35,48,49</sup> Knowledge of Sn isotope signatures of terrestrial rocks is still limited due to the scarcity of high-quality isotope data for igneous rocks, and there has been no community-recognized certified international Sn isotopic reference material. In this study, we developed a double-spike Sn isotope analytical method that can be applied to various geological materials, and we reported high-precision Sn concentrations and isotopic data for a wide range of geological reference materials.

## 2. Double spike design

Sample standard bracketing method and element doping can be used for mass bias correction during Sn isotope analysis by MC-ICP-MS.<sup>50,51</sup> However, Sn is volatile during sample dissolution, and vaporization loss of Sn could induce Sn isotope fractionation,<sup>47,52–54</sup> compromising the accuracy of the Sn isotope analysis. Only the double spike method could rigorously correct the mass-dependent isotope fractionation processes that occur during sample processing, chromatographic purification, and mass spectrometry, given that the spike had been

equilibrated with the sample prior to these processes.<sup>51</sup> This method involves the measurement of isotope data for the mixture of the sample of interest with a well-calibrated double spike containing two enriched isotopes compared to natural abundance.<sup>36</sup> Tin has more than four stable isotopes and is a suitable candidate for the application of the double spike technique for mass bias correction.

The selection of the double spike combination is based on the following criteria: (1) the spike isotopes are not susceptible to potential interferences, (2) the spike combination fits the cup configuration and mass dispersion of the mass spectrometer, and (3) the spike combination is associated with minimum systematic errors in double-spike inversion. The low abundance isotopes of tin (<sup>112</sup>Sn, <sup>114</sup>Sn, <sup>115</sup>Sn) are susceptible to interferences of Cd and In, thus they are not considered.<sup>37,44</sup> The isotopes of <sup>116</sup>Sn, <sup>119</sup>Sn, and <sup>124</sup>Sn could also suffer from potential elemental and molecular interference from neighboring elements (Cd, Te, Mo, Ag) if they are not well-separated.<sup>41,43,44</sup> Several spike assemblages, including <sup>117</sup>Sn–<sup>122</sup>Sn and <sup>117</sup>Sn–<sup>119</sup>Sn double spikes, had been used in previous studies.<sup>41,42,44</sup> <sup>117</sup>Sn–<sup>122</sup>Sn is preferred for the tolerance of a range of sample/spike ratios. Based on these considerations, we chose to use <sup>117</sup>Sn–<sup>122</sup>Sn double spike with <sup>117</sup>Sn–<sup>118</sup>Sn–<sup>120</sup>Sn–<sup>122</sup>Sn inversion and <sup>118</sup>Sn as the denominator (Fig. 1), and simulations from the “double spike toolbox”<sup>55</sup> show that this combination maintains minimal systematic errors over a spike/(spike + sample) ratio range of 0.2 to 0.65 (Fig. 2).

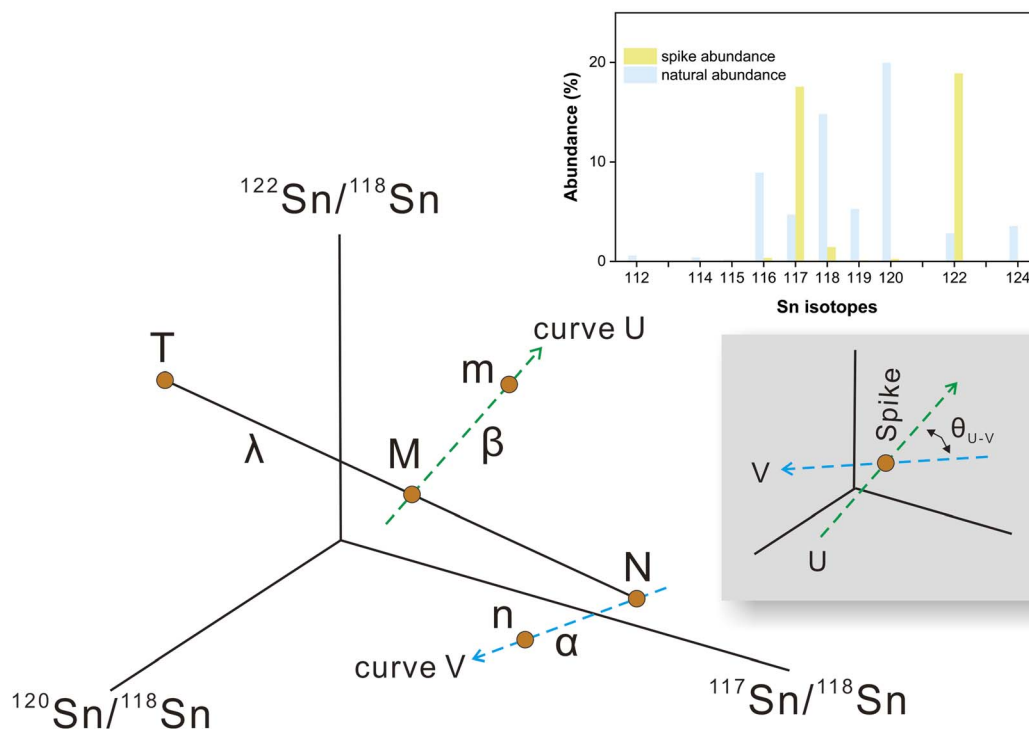


**Fig. 1** Schematic diagram showing the principle of the double-spike Sn isotope method. The natural sample (N) and double spike (T) in the four-isotope space have different compositions. A mixture of natural sample and spike lies on the T–M–N mixing line with the mixing proportion of  $\lambda$ . The measured composition of the mixture and natural sample is fractionated along the instrumental fractionation line (curve U and V) with the fractionation factors  $\alpha$  and  $\beta$ .  $\theta_{U-V}$  represents the intersection angle of curve U and curve V. The relative abundances of the sample and spike are also shown for the optimal spike-to-sample ratio.

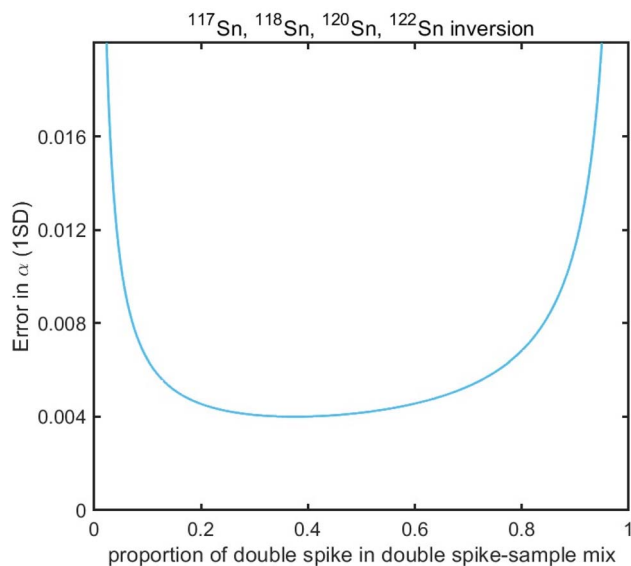


Fig. 2 Theoretical error in  $\alpha$  as a function of spike proportions in spike-sample mixtures with  $^{117}\text{Sn}$ – $^{122}\text{Sn}$  double spike using  $^{117}\text{Sn}$ – $^{118}\text{Sn}$ – $^{120}\text{Sn}$ – $^{122}\text{Sn}$  inversion.

The Sn double spike was prepared as a mixture of two concentrated spike solutions. Two Sn metal ingots enriched in  $^{117}\text{Sn}$  and  $^{122}\text{Sn}$  respectively were purchased from Isoflex (<https://www.isoflex.com>). The spikes were carefully weighed and transferred to Teflon beakers for digestion with HCl. The double spike solution was prepared by mixing the two individual spikes properly to achieve a composition of approximately 53%  $^{117}\text{Sn}$  and 47%  $^{122}\text{Sn}$ . The double spike solution was stored in 1 M HCl at a concentration of  $400 \mu\text{g g}^{-1}$  as a stock solution to be diluted for further isotope measurements.

The accuracy and repeatability of double spike data rely on the correct calibration of the spike compositions relative to the

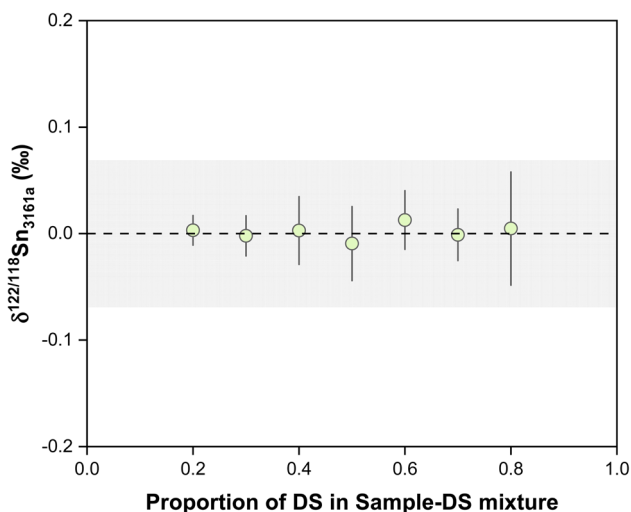


Fig. 3 The plot shows the results of double-spike calibrations. The dashed line and shaded box represent the theoretical value and external reproducibility of the double spike method. All uncertainties on individual data points reflect the 2SD of the samples.

primary isotope standard. The double spike was calibrated by measuring a series spike-NIST 3161a mixture, with the spike proportion increasing gradually from pure standard to pure spike. The double spike composition is determined relative to the NIST 3161a standard following the approach of Klaver and Coath.<sup>56</sup> A series of spike-standard mixtures, with the proportions of double spike varying from 0.2 to 0.8, were used to define the standard-spike mixing line and ensure the quality of the calibration. If the calibration is correct, the result for mixtures of different spike proportions should yield consistent close to zero results, which is illustrated in Fig. 3. For spike/(spike + sample) proportion within the range of 0.2 to 0.8, the accuracy of the double spike method is insensitive to the effect of the spike-to-sample ratio.

### 3. Experimental methods

#### 3.1. Materials and reagents

All chemical treatments of samples were performed in an ISO Class 6 clean room with ISO Class 5 fume hoods at the State Key Laboratory for Mineral Deposits Research, Nanjing University. The semiconductor-grade acids (HCl,  $\text{HNO}_3$ , HF) were purchased and used for all sample preparation and ion-exchange chromatography. Teflon beakers are soaked in 4.5 M nitric acid and then refluxed with concentrated  $\text{HNO}_3$ –HF mixture and HCl at  $130^\circ\text{C}$  for at least one day, then rinsed with ultrapure water (resistivity of  $18.2 \text{ M}\Omega \text{ cm}^{-1}$ ) before usage. Commercially available  $100 \mu\text{g g}^{-1}$  multi-element stock solutions for column calibrations were supplied by Aladdin® (Lot #C2011). The single-element Sn standard solution used for quantitative analysis was purchased from Macklin® (Lot #C10053783,  $1000 \mu\text{g g}^{-1}$ ). Since there have been no community-recognized international Sn isotopic reference materials, several  $100 \mu\text{g mL}^{-1}$  pure Sn elemental standard solutions, including NIST 3161a (Lot #140917), SPEX (Lot #22-19SNY), and  $\text{SnCl}_4$  solutions, were used as in-house standards. Eight USGS and one Chinese geological reference materials, including basalts (BCR-2, BHVO-2, BIR-1), andesite (AGV-2), granites (GSP-2, JG-2, GSR-1), rhyolite (RGM-1), and marine sediment (NOD-A-1), were processed and analyzed to assess the accuracy and intermediate precision of our chemical and mass spectrometric procedures. These geological reference materials were selected to represent a wide spectrum of sample matrices.

#### 3.2. Sample preparation and digestion

Based on bulk rock concentration data, approximately 100 to 1000 mg of rock powders (containing 1–2  $\mu\text{g}$  Sn) were digested in a tightly capped Teflon beaker with 8 mL 1:1 mixture of  $\text{HNO}_3$ –HF on a hotplate at  $130^\circ\text{C}$ . Before digestion, the sample was mixed with a  $^{117}\text{Sn}$ – $^{122}\text{Sn}$  double spike solution at an optimal spike-to-sample ratio of 39:61. Initial digestion lasted for two days, during which the Sn dissolved from the rock powders was equilibrated with the double spike, then the solution was evaporated to dryness at  $80^\circ\text{C}$  and re-dissolved in 6 mL aqua regia and dried. After that, the sample was dissolved in 8 mL concentrated HCl to reflux at  $130^\circ\text{C}$  for two days to

dissolve fluorides before drying again at 80 °C. About 100 µL HF was added to fix Sn before each evaporation step to prevent Sn loss by volatilization or hydrolysis. Afterwards, the sample was re-dissolved in 0.5 M HCl as required to be loaded on the column for Sn purification.

### 3.3. Column chemistry

The chemical separation of Sn used as the default method in this study was performed with 1.5 mL bed volume Eichrom TRU resin filled in Biorad plastic columns. The ion exchange

chromatography method used in this study was similar to those reported by Creech *et al.*<sup>42</sup> The resin was pre-cleaned sequentially with H<sub>2</sub>O, 0.5 M HCl, and 0.5 M HNO<sub>3</sub> after resin loading and then conditioned with 0.5 M HCl (for details, see Table 1). After sample loading, the matrix elements were eluted with 0.5 M and 0.25 M HCl. Then Sn was recovered using an eluent of 12 mL 0.5 M HNO<sub>3</sub>. 100 µL of concentrated HF was added to the collection beaker to prevent Sn hydrolysis before the collection of Sn cut. Subsequently, the purified Sn fractions were dried down at 80 °C and were taken up again in 0.3 M HNO<sub>3</sub> and 0.006 M HF.

A two-stage column procedure with a second (additional) anionic chloride form AG1-X8 resin following Friebel *et al.*<sup>43</sup> was also evaluated in this study. The elution steps for the second stage of chemistry are summarized in Table 1. After the first stage column treatment, the sample was loaded onto the second stage column with 10 mL 1 M HCl. Then the column was eluted with another 20 mL 1 M HCl, 10 mL 6 M HCl, and 2 mL 1 M HNO<sub>3</sub>.

### 3.4. Mass spectrometry

All double spike Sn isotope analysis was performed on a Nu 1700 Sapphire MC-ICP-MS at the State Key Laboratory for Mineral Deposits Research and Frontiers Science Center for Critical Earth Material Cycling, Nanjing University. The detailed instrument settings and operational parameters for data acquisition are summarized in Table 2. During Sn isotope analysis, Sb isotopes (<sup>123</sup>Sb, <sup>125</sup>Sb) were measured for mass bias correction when applicable. The signals of <sup>125</sup>Te and <sup>111</sup>Cd were measured along with Sn isotopes to monitor the effects of isobaric interferences from Te and Cd on Sn isotopes (*i.e.*, <sup>124</sup>Te, <sup>122</sup>Te, <sup>120</sup>Te on <sup>124</sup>Sn, <sup>122</sup>Sn, and <sup>120</sup>Sn, respectively; <sup>116</sup>Cd on <sup>116</sup>Sn) (Table S1†).

For double spike Sn isotope analysis, the concentration of all solutions was adjusted to 100 ng g<sup>-1</sup> in a mixed acid of 0.3 M HNO<sub>3</sub> and 0.006 M HF, except for acidity tests. The sample was introduced into the ICP *via* an Aridus III desolvator with a 100

Table 1 Chromatographic procedure for the separation of Sn using TRU and AG1-X8 resin

| Step  | Eluant                 | Volume/mL |
|---|------------------------|-----------|
| <b>1.5 mL TRU resin (100–150 mesh)</b>        |                        |           |
| Cleaning                                      | H <sub>2</sub> O       | 5         |
|   | 0.5 M HCl              | 5         |
|   | H <sub>2</sub> O       | 5         |
|   | 0.5 M HNO <sub>3</sub> | 5         |
|   | H <sub>2</sub> O       | 5         |
|   | 0.5 M HNO <sub>3</sub> | 5         |
| Conditioning                                  | H <sub>2</sub> O       | 5         |
| Loading                                       | 0.5 M HCl              | 4         |
| Matrix elution                                | 0.5 M HCl              | 2         |
|   | 0.5 M HCl              | 4         |
| Sn collection<br>(with 100 µL HF added first) | 0.25 M HCl             | 7         |
|   | 0.5 M HNO <sub>3</sub> | 12        |
| <b>2 mL AG1-X8 resin (100–200 mesh)</b>       |                        |           |
| Cleaning                                      | H <sub>2</sub> O       | 5         |
|   | 1 M HNO <sub>3</sub>   | 10        |
| Conditioning                                  | 1 M HCl                | 10        |
| Loading                                       | 1 M HCl                | 10        |
| Matrix elution                                | 1 M HCl                | 20        |
|   | 6 M HCl                | 10        |
|   | 1 M HNO <sub>3</sub>   | 2         |
| Sn collection (with 100 µL HF added first)    | 1 M HNO <sub>3</sub>   | 10        |

Table 2 Instrumental operation parameters for Sn isotopic measurement using a Nu 1700 Sapphire MC-ICP-MS

| Parameter                    | Value                                  |                         |                         |                         |                         |                         |                         |                         |                         |                         |                         |                         |
|------------------------------|--|-------------------------|-------------------------|-------------------------|-------------------------|-------------------------|-------------------------|-------------------------|-------------------------|-------------------------|-------------------------|-------------------------|
| RF power                     | 1300 W                                 |                         |                         |                         |                         |                         |                         |                         |                         |                         |                         |                         |
| Auxiliary gas flow rate      | 1 L min <sup>-1</sup>                  |                         |                         |                         |                         |                         |                         |                         |                         |                         |                         |                         |
| Sample gas flow rate         | 0.9 L min <sup>-1</sup>                |                         |                         |                         |                         |                         |                         |                         |                         |                         |                         |                         |
| Plasma cooling gas flow rate | 13 L min <sup>-1</sup>                 |                         |                         |                         |                         |                         |                         |                         |                         |                         |                         |                         |
| Measurement mode             | Static                                 |                         |                         |                         |                         |                         |                         |                         |                         |                         |                         |                         |
| Interface cones              | Standard Ni cones                      |                         |                         |                         |                         |                         |                         |                         |                         |                         |                         |                         |
| Acceleration voltage         | ~6000 V                                |                         |                         |                         |                         |                         |                         |                         |                         |                         |                         |                         |
| Detector                     | Faraday cups                           |                         |                         |                         |                         |                         |                         |                         |                         |                         |                         |                         |
| Amplifier                    | 10 <sup>11</sup> Ω                     |                         |                         |                         |                         |                         |                         |                         |                         |                         |                         |                         |
| Sample measurement time      | 40 × 3 s integrations                  |                         |                         |                         |                         |                         |                         |                         |                         |                         |                         |                         |
| Instrument resolution        | 5258                                   |                         |                         |                         |                         |                         |                         |                         |                         |                         |                         |                         |
| Nebulizer                    | MicroFlow PFA-100 µL min <sup>-1</sup> |                         |                         |                         |                         |                         |                         |                         |                         |                         |                         |                         |
| Sample introduction system   | Aridus III                             |                         |                         |                         |                         |                         |                         |                         |                         |                         |                         |                         |
| Aridus Ar sweep gas          | 5.65 L min <sup>-1</sup>               |                         |                         |                         |                         |                         |                         |                         |                         |                         |                         |                         |
| Solution concentration       | 100 ng mL <sup>-1</sup>                |                         |                         |                         |                         |                         |                         |                         |                         |                         |                         |                         |
| Cup configuration            | H7<br><sup>125</sup> Te                | H6<br><sup>124</sup> Sn | H5<br><sup>123</sup> Sb | H4<br><sup>122</sup> Sn | H3<br><sup>121</sup> Sb | H2<br><sup>120</sup> Sn | H1<br><sup>119</sup> Sn | Ax<br><sup>118</sup> Sn | L1<br><sup>117</sup> Sn | L2<br><sup>116</sup> Sn | L3<br><sup>115</sup> Sn | L4<br><sup>114</sup> Cd |

$\mu\text{L min}^{-1}$  PFA nebulizer. The data acquisition sequence consists of 40 seconds of sample uptake time and forty cycles of three seconds of signal integration on Faraday cups. The typical signal intensity for  $^{120}\text{Sn}$  was  $\sim 12\text{ V}$  per  $\mu\text{g g}^{-1}$ . Measurement of blanks was performed at the beginning of every session and corrected for both standards and samples. Between each isotope analysis, the sample introduction system was washed through uptaking  $0.3\text{ M HNO}_3$  and  $0.006\text{ M HF}$  solutions sequentially from three tubes, each for 40 seconds, to suppress the memory effect and bring the background to the pre-analysis level. The  $^{120}\text{Sn}$  background was measured to be lower than  $9\text{ mV}$  after the three-step rinsing, which was  $>1000$  times lower than the sample signal. Every sample was bracketed by a spiked NIST 3161a standard at the same concentration in an analytical session.

To validate the double spike method, several in-house standard Sn solutions were measured using elemental doping and sample-standard bracketing under wet plasma conditions. For this analysis, the  $1\text{ }\mu\text{g g}^{-1}$  Sn solution was doped with  $300\text{ ng g}^{-1}$  Sb and was introduced into ICP with a standard glass spray chamber *via* a  $100\text{ }\mu\text{L min}^{-1}$  PFA nebulizer. The Faraday cup configuration was the same as the double spike method (Table 2). Data reduction of Sn isotope analysis for this method was similar to a previous study.<sup>52</sup> All isotopic results are expressed as  $\delta^{122/118}\text{Sn}$  notation relative to the primary Sn isotopic reference solution NIST 3161a in this study, which is  $\delta^{122/118}\text{Sn} = [({}^{122}\text{Sn}/{}^{118}\text{Sn})_{\text{sample}}/({}^{122}\text{Sn}/{}^{118}\text{Sn})_{3161a} - 1] \times 1000$ .

## 4. Results and discussion

### 4.1. Separation and isotope fractionation of Sn during ion exchange column chemistry

High-precision Sn isotope analysis, with or without a double spike, could be compromised by the isobaric and molecular interference of Te, Cd, In, and  $\text{Mo}^{41}$  (Table S1†), thus these elements need to be effectively separated from Sn during the column chemistry that is aimed at purifying Sn from the rock matrix. In the literature, different resins, including TBP, AG MP-1, and AG1-X8, had been used for the purification of Sn,<sup>25,30,41,43,44,57,58</sup> more recently, several studies have utilized TRU resin for the Sn separation procedure.<sup>1,30,41–43,48,59</sup>

The elution curves of different elements for the two different column procedures are shown in Fig. 4. For the TRU resin, the majority of matrix elements were eluted off the column completely with  $0.5\text{ M HCl}$ , whereas In was released from the column during the elution of  $0.25\text{ M HCl}$ . Then Sn was recovered by the elution of  $0.5\text{ M HNO}_3$ . Although a previous study stated that Bi, In, and Mo could not be separated well from Sn with TRU resin,<sup>44</sup> our results show that the In/Sn ratio was lower than  $0.007$  and the  $[\text{X}]/[\text{Sn}]$  ratio of Bi, and Mo was lower than  $0.001$  after this stage of column chemistry for all igneous rocks. The yield of Sn by the treatment of TRU resin in this study was measured to be  $99.8 \pm 0.3\%$  ( $2\text{SD}$ ,  $N = 3$ ). For comparison, AG1-X8 is an anion exchange resin that can separate Sn from a number of matrix elements, including Fe, Mg, Mo, In, and Cd.<sup>30,43,44</sup> Various elements, including In and Pb, could be eluted off the column before the Sn cut, but the full separation of Sn,

Cd, and Zn cannot be achieved. In this step, the recovery of Sn was  $99.1 \pm 2.5\%$  ( $2\text{SD}$ ,  $N = 2$ ). The procedural blank from the dissolution and the two-stage column chemistry is lower than  $5.6\text{ ng}$ , contributing to less than  $0.3\%$  of the analyzed samples.

Ion-exchange processes on chromatography columns are known to fractionate stable isotopes of Fe, Ga, Cu, Zn, Mo, and Ca.<sup>60–64</sup> No Sn isotope fractionation was measured in previous studies involving TRU resin when the Sn recovery was above  $94\%$ .<sup>32,48,65</sup> However, a significant Sn isotope offset after column chemistry was reported by Yamazaki *et al.*,<sup>66</sup> which was thought to originate from the incomplete recovery or matrix effects. Therefore, it is important to assess the effect of incomplete recovery during ion-exchange column chemistry on Sn isotopes. This was done by double spike analysis of the different Sn fractions of the elution curve, as shown in Fig. 5. Remarkable Sn isotope fractionation occurred on the TRU ion-exchange column. The Sn (original  $\delta^{122/118}\text{Sn}_{3161a} = -0.095 \pm 0.030\%$ ) that was firstly eluted off the TRU resin was isotopically heavier than the bulk Sn solution, implying that the resin held lighter Sn isotopes at the beginning. The light Sn isotopes were eluted off the column immediately after the peak of the elution curve (Fig. 5). Specifically, the majority of Sn (around  $93\%$ ) cuts show a decreasing trend with  $\delta^{122/118}\text{Sn}_{3161a}$  varying from  $0.218 \pm 0.073\%$  to  $-0.570 \pm 0.042\%$ , similar to Ca and Fe isotopes.<sup>60,61</sup> However, the Sn eluted off the column as the tail of the elution curve became isotopically heavier again (Table S2†). The  $\delta^{122/118}\text{Sn}_{3161a}$  for the remaining Sn (around  $6\%$ ) cuts increased from  $-0.570 \pm 0.042\%$  to  $1.138 \pm 0.053\%$ . The origin of this phenomenon (*v*-shaped  $\delta^{122/118}\text{Sn}$  value for the Sn elution curve) is unclear but could be due to the transition of Sn species during the elution by  $\text{HNO}_3$ . Based on the detailed elemental data from the elution curve, it is estimated that a  $3\%$  Sn loss (not collected) from the resin could cause an Sn isotope fractionation by  $0.025\%$  in  $\delta^{122/118}\text{Sn}$ , although we note that such an isotopic effect is corrected by the double spike method.

### 4.2. Double spike data inversion

Cadmium and Te are the main issues of concern during Sn isotope measurements as they form isobaric interferences on  $^{116}\text{Sn}$ ,  $^{122}\text{Sn}$ , and  $^{124}\text{Sn}$ . We monitored  $^{111}\text{Cd}$  and  $^{125}\text{Te}$  to correct the effect of these elemental interferences before conducting double spike data inversion, following the convention of previous studies.<sup>44,67</sup> During Sn isotope analysis for geological samples, however, we found that the measured  $^{125}\text{Te}$  intensities stayed constant at a level below  $1.5\text{ mV}$  for all samples, and the signal for  $^{111}\text{Cd}$  was always lower than  $0.7\text{ mV}$ . The results show no obvious difference with and without correction for the elemental interference of Te and Cd.

The reduction of double-spike data can be achieved with a variety of methods, including Nest iteration,<sup>68,69</sup> geometric method,<sup>70,71</sup> and Newton–Raphson iteration approaches.<sup>51,55</sup> All the data reduction of this study was performed using a double spike toolbox<sup>55</sup> with a MATLAB<sup>®</sup> code following the Newton–Raphson iteration approach. The inputs of the inversion include the measured intensities of all the isotopes for samples and the calibrated double-spike composition. To correct for

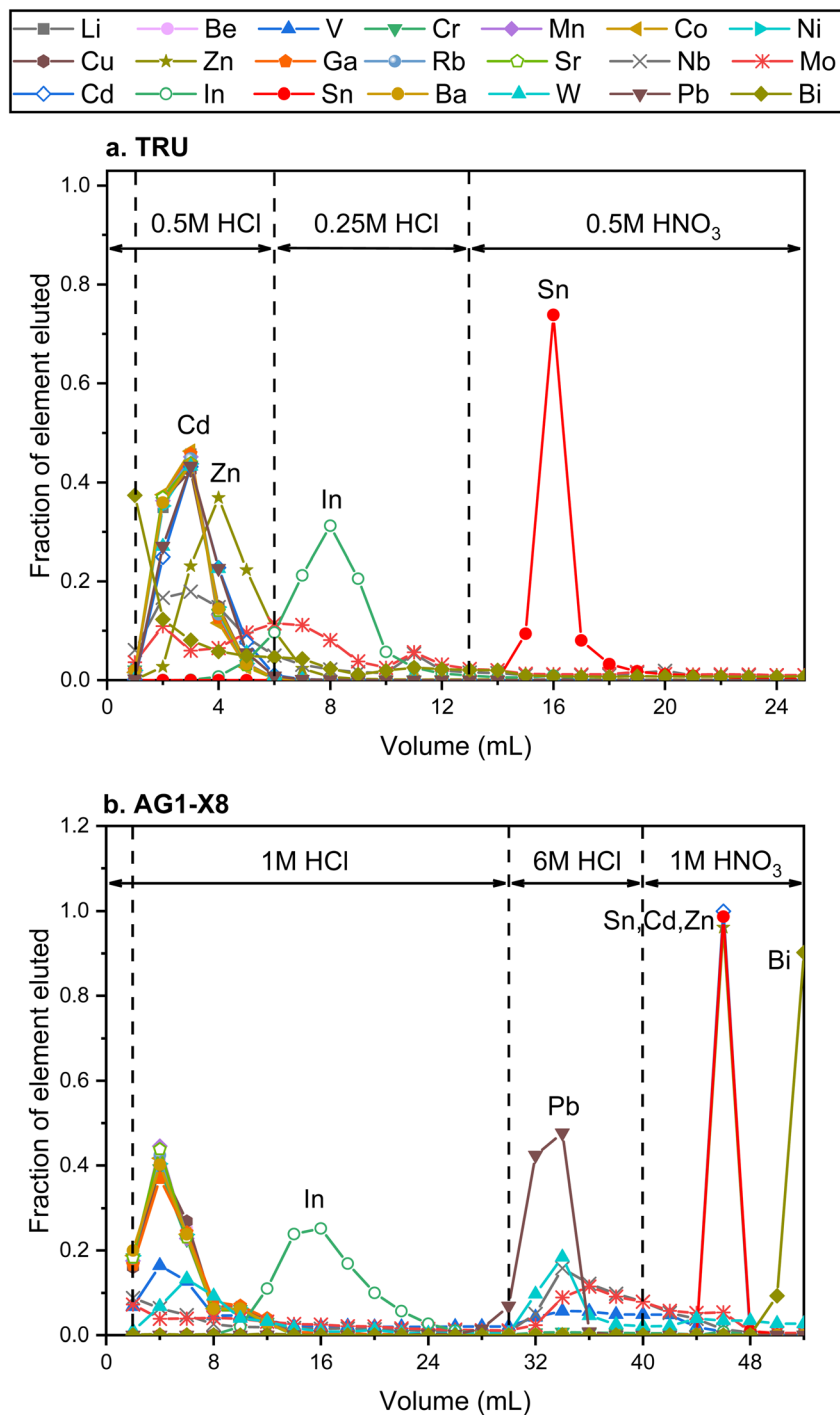


Fig. 4 Elution curves of the Sn purification procedure using different reagents. (a) and (b) Represent the elution curves using TRU resin and AG1-X8 resin, respectively.

potential deviations from the exponential law and shift of the gains for Faraday collectors during the measurements,<sup>42,44</sup> a bracketing standard was used to normalize isotopic values after a double spike inversion of each sample.<sup>44,72-77</sup> Therefore, all the data are reported as the deviation of  $\delta^{122/118}\text{Sn}$  of a sample relative to the average  $\delta^{122/118}\text{Sn}$  of two bracketing spiked NIST 3161a, similar to Wang *et al.*<sup>44</sup> The geometrical method was also used for comparison using MATLAB<sup>®</sup>, and

consistent results were found, for which the details are provided in the ESI A.†

#### 4.3. Effects of acidity and concentration mismatch

The effect of acid mismatch has been reported on K, Fe, and Ba isotope measurements by MC-ICP-MS using sample standard bracketing methods.<sup>78,79</sup> The impact of the acid concentration mismatch between the samples and standards on the accuracy

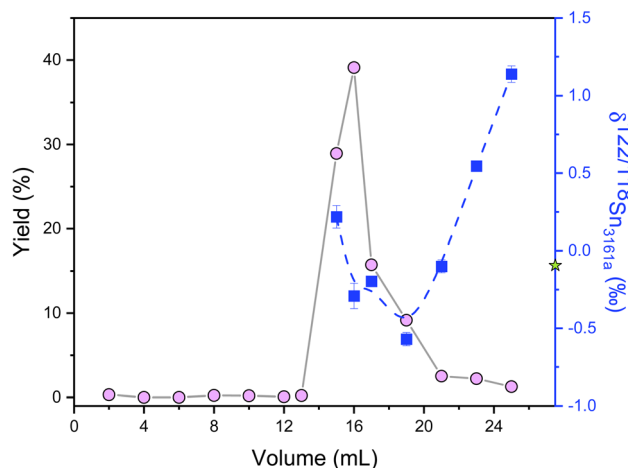


Fig. 5  $\delta^{122/118}\text{Sn}_{3161a}$  values of Sn cuts of a laboratory elemental solution eluted from the column with TRU resin. The circles represent the fractions of Sn, and the squares indicate Sn isotope values of corresponding fractions. The solid and dashed lines are just shown for visual guidance. The star denotes the  $\delta^{122/118}\text{Sn}_{3161a}$  composition of loading Sn solution. All uncertainties on individual data points reflect the 2SD of the samples.

of Sn isotope analysis was evaluated by analyzing the NIST 3161a in various acid matrices. Spiked NIST 3161a solutions were diluted in  $\text{HNO}_3$ -HF at various concentrations and analyzed against the NIST 3161a solution in 0.3 M  $\text{HNO}_3$  and 0.006 M HF. The results show no Sn isotopic deviation for the spiked NIST 3161a analyzed at different acid concentrations (Fig. 6a), indicating that Sn isotope measurements are insensitive to the different acid concentrations between bracketing standards and samples using our double spike method.

Previous studies reported analytical inaccuracy when there was a mismatch in the concentration of the sample and standard during the double spike analysis of Cd and Se isotopes and sample-standard-bracketing analysis of K and Ba stable isotopes.<sup>80–83</sup> The effect of intensity mismatch on Sn isotope

analysis was evaluated by analyzing spiked NIST 3161a solutions of concentrations varying from 20 to 150  $\text{ng g}^{-1}$  against the spiked NIST 3161a bracketing standard with a constant concentration of 100  $\text{ng g}^{-1}$  Sn. Both the bracketing standards and samples were prepared from a 1  $\mu\text{g g}^{-1}$  spiked NIST 3161a stock solution. The concentrations are calculated based on the total Sn intensities of all measured Sn isotopes. The measured  $\delta^{122/118}\text{Sn}$  values are plotted in Fig. 6b as a function of the ratio between the Sn concentration of the sample analyzed and the NIST 3161a standard. The results show that the measured  $\delta^{122/118}\text{Sn}_{3161a}$  values decrease with increasing Sn concentrations following a curved relationship. When the Sn concentration of the sample is 20% of the standard (*i.e.*,  $I_{\text{sample}}/I_{\text{standard}} = 0.2$ ), the inaccuracy in the measured  $\delta^{122/118}\text{Sn}_{3161a}$  is up to 0.45‰. For sample/standard Sn concentration ratios lower than 0.4, we can observe an obvious offset of  $\delta^{122/118}\text{Sn}_{3161a}$  relative to the bracketing standard (Fig. 6b). It is necessary to maintain a sample concentration of 80 to 120  $\text{ng g}^{-1}$  to ensure accurate and precise results for the protocol in this study. We note that the effect of concentration mismatch is likely relevant to instrumental and double spike settings and may differ between different laboratories.

#### 4.4. Matrix effects

Elements other than the target element may affect the transport of the analyte in the ICP and the ion extraction in the interface, causing matrix effects.<sup>81,83</sup> Abnormal isotopic results could also arise due to molecular and isobaric interferences caused by matrix elements.<sup>80</sup> Although column chemistry was developed to purify the target elements from matrix elements, elements like Mg, Fe, and Ca are common and major elements in geological matrices. As also pointed out by previous studies, the existence of matrix elements such as U, Ag, Ru, Mo, and Cd in the Sn solution could lead to various interferences on Sn isotopes on MC-ICP-MS.<sup>41,84</sup> The possible molecular, doubly charged, and isobaric interferences on Sn isotopes are summarized in Table S1.† To evaluate the matrix effects on Sn

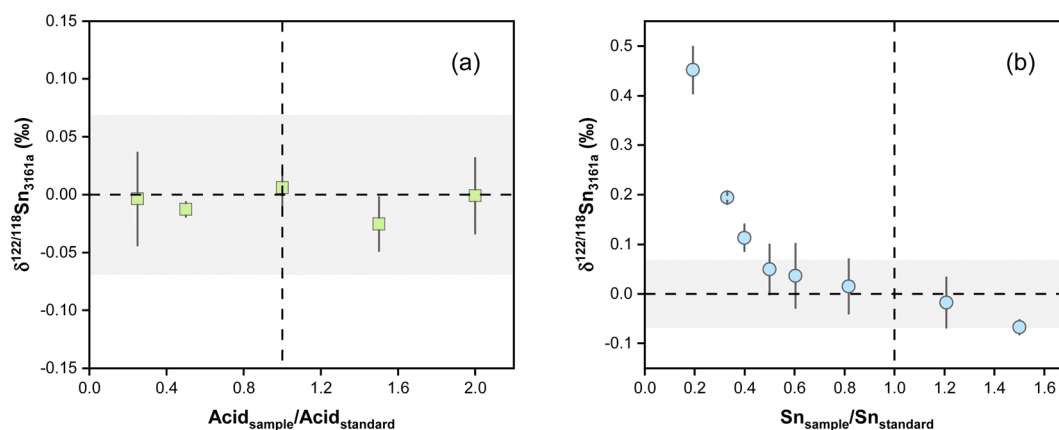


Fig. 6 (a)  $\delta^{122/118}\text{Sn}_{3161a}$  variations with different acid concentrations. The NIST 3161a standards used a 0.3 M  $\text{HNO}_3$  to 0.006 M HF acid matrix. The acid strength was changed by the dilution of an acid mixture with 0.6 M  $\text{HNO}_3$  and 0.012 M HF. (b) The effect of Sn concentration mismatches between the sample and standard on  $\delta^{122/118}\text{Sn}_{3161a}$  analysis. The dashed lines and shaded boxes represent the true value and external reproducibility. The error bars (2SD) are based on at least two replicate measurements.

isotope measurements, we doped a series of matrix elements (Mg, Ca, Fe, Ti, Ni, As) to a spiked NIST 3161a Sn solution at the mass ratios of  $[X]/[Sn]$  ( $\text{ng g}^{-1}/\text{ng g}^{-1}$ ) varying from 0.01 to 0.5. These matrix-doped Sn solutions were then measured against spiked pure NIST 3161a Sn. The results are shown in Fig. 7. We also doped U, Ag, Ru, Mo, and Cd into the spiked NIST 3161a Sn solution to quantitatively evaluate the effects of elements that might cause molecular and isobaric interferences. Our results demonstrate that the presence of U, Ag, Ru, and Mo below 50% of Sn causes a negligible effect on the accuracy of Sn isotope analysis with the double spike method; these results show that the double spike method is effective in correcting mass bias in

the instrument even if the mass bias may vary due to the existence of matrix elements.

However, we found that  $\text{Cd}/\text{Sn} > 0.01$  ( $^{111}\text{Cd}$  up to 68 mV for our setting) in sample solutions would cause obvious offset on the Sn isotope measurements (Fig. 8). Such a deviation did not originate from the isobaric interference of  $^{116}\text{Cd}$  on  $^{116}\text{Sn}$ , as the four isotopes for double spike inversion are  $^{117}\text{Sn}$ ,  $^{118}\text{Sn}$ ,  $^{120}\text{Sn}$ , and  $^{122}\text{Sn}$ . We speculate that the observed analytical inaccuracy was caused by the formation of cadmium hydride,<sup>85,86</sup> specifically, the interference of  $^{116}\text{Cd}^1\text{H}^+$  on  $^{117}\text{Sn}^+$ . We performed the correction of  $^{116}\text{Cd}^1\text{H}^+$  on  $^{117}\text{Sn}^+$  by assuming different production rates of cadmium hydride. The results are

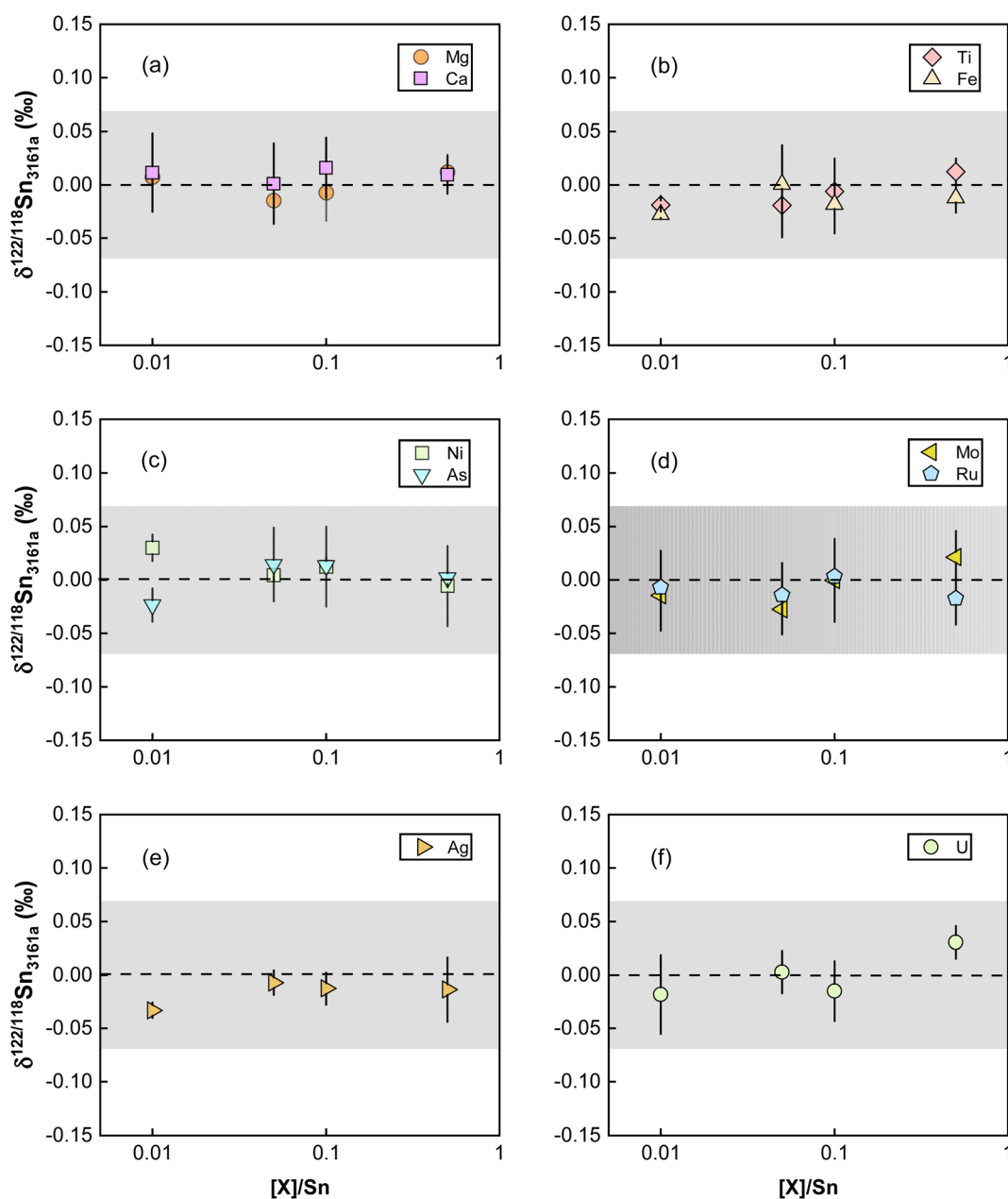


Fig. 7 Doping experiments for testing the effect of matrix elements with and without interferences on Sn isotope measurements. The dashed line and shaded box represent the true theoretical value and external error for the double spike method of this study. All uncertainties on individual data points reflect the 2SD of the samples.

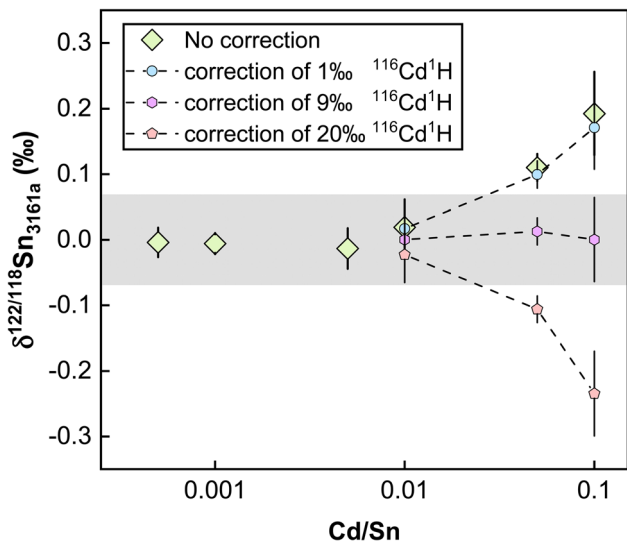


Fig. 8 Doping experiments for Cd to test the effect of its interferences on Sn isotope measurements. The dots with dashed lines denote the correction of  $^{116}\text{Cd}^1\text{H}$ , with the numbers signifying the productivity relative to  $^{116}\text{Cd}$ . The shaded box represents the true value for the double spike method of this study. All uncertainties on individual data points reflect the 2SD of the samples.

summarized in Fig. 8, which shows that when a production rate of 0.9% is assumed for cadmium hydride from cadmium ion, the influence of Cd can be corrected. We note that such a production rate of cadmium hydride could vary between different analytical sessions or experimental settings, thus, the safe protocol would be to ensure that Cd/Sn is lower than 0.01 for sample analysis.

#### 4.5. Repeatability and intermediate precision

Different pure reference materials have been used in previous Sn isotope studies, including Johnson-Matthey Puratronic Sn,<sup>39</sup> SPEX Sn standard solution in  $\text{HNO}_3$  (Lot #CL5-45SN,<sup>66,87</sup> Lot #CL8-02SNY,<sup>88</sup> Lot #CL6-83SNY<sup>43</sup>), SPEX Sn standard solution in HCl (Lot #14-84SN,<sup>66,87</sup> Lot #20-168SNY,<sup>88</sup> Lot #22-19SNY<sup>52</sup>), NIST 3161a (Lot #070330,<sup>41,43,44,47,66,87</sup> Lot #140917 (ref. 52)), Sn\_IPGP,<sup>42</sup> and NCS Sn.<sup>41</sup> The isotopic homogeneity of these reference solutions between different batch numbers has not

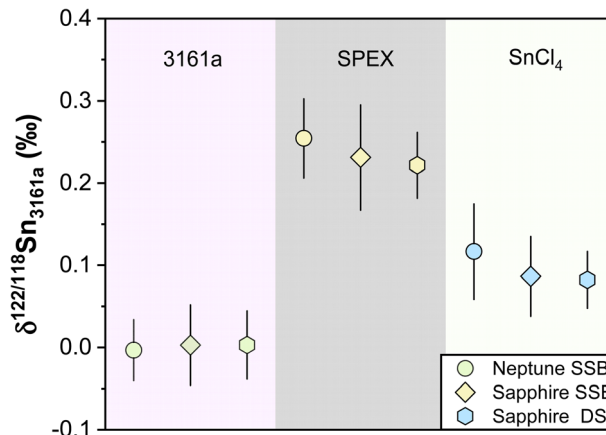


Fig. 9  $\delta^{122/118}\text{Sn}_{3161a}$  values of pure laboratory solutions of NIST 3161a, SPEX, and  $\text{SnCl}_4$  during the past half years. The data of Neptune SSB are from She *et al.*<sup>52</sup> The Sapphire SSB and DS indicate the data measured with Nu Sapphire 1700 using both sample standard bracketing and double spike methods. All uncertainties on individual data points reflect the 2SD of the samples.

been verified. In this study, three in-house standard solutions were repeatedly measured. The  $\delta^{122/118}\text{Sn}_{3161a}$  compositions for our NIST 3161a, SPEX, and  $\text{SnCl}_4$  using the sample standard bracketing (SSB) method are consistent with our double spike (DS) method (Table 3) (Fig. 9). These values, measured on the Nu 1700 Sapphire MC-ICP-MS, are also consistent with those that were measured on a Neptune plus MC-ICP-MS as reported in our previous study,<sup>52</sup> (Fig. 9). We obtained a long-term intermediate precision of better than  $\pm 0.041\text{‰}$  based on these in-house reference solutions. We also measured the NIST 3161a from ETH with a different batch number (#070330) with SSB and DS methods, which was indistinguishable from our primary standard (Table 3).

To ensure that the chemical purification process does not introduce inaccuracy for Sn isotope measurements, we processed pure and synthetic spiked solutions with our column chemistry, and analyzed them as unknowns using SSB and DS methods. We processed two pure solutions of NIST 3161a and  $\text{SnCl}_4$  with column chemistry, confirming that no resolvable Sn isotope fractionation was induced by column chemistry (Table

Table 3 The  $\delta^{122/118}\text{Sn}_{3161a}$  composition of pure reference materials analyzed by different methods

|                          | $\delta^{122/118}\text{Sn}$ (‰) | Neptune SSB <sup>a</sup> |       |          | Sapphire DS |     |          |       |    |
|--------------------------|---------------------------------|--------------------------|-------|----------|-------------|-----|----------|-------|----|
|                          |                                 | 2SD                      | 2SD   | <i>N</i> | 2SD         | 2SD | <i>N</i> |       |    |
| Without column chemistry | NIST 3161a (#140917)            | -0.003                   | 0.037 | 0.003    | 0.049       | 21  | 0.003    | 0.041 | 25 |
|                          | SPEX (#22-19SNY)                | 0.254                    | 0.048 | 0.231    | 0.064       | 51  | 0.222    | 0.040 | 31 |
|                          | $\text{SnCl}_4$                 | 0.117                    | 0.058 | 0.086    | 0.048       | 18  | 0.082    | 0.034 | 17 |
| With column chemistry    | NIST 3161a (#070330)            |                          |       | 0.017    | 0.056       | 6   | -0.013   | 0.049 | 11 |
|                          | NIST 3161a (#140917)            |                          |       | -0.011   | 0.059       | 3   | 0.001    | 0.006 | 3  |
|                          | NIST 3161a (#140917)            |                          |       |          |             |     | 0.005    | 0.027 | 3  |
|                          | NIST 3161a (#140917) + matrix   |                          |       |          |             |     | 0.012    | 0.023 | 3  |
|                          | Evaporated NIST 3161a (#140917) |                          |       | 0.224    | 0.044       | 3   |          |       |    |
|                          | $\text{SnCl}_4$                 |                          |       | 0.141    | 0.085       | 3   |          |       |    |

<sup>a</sup> The data of Neptune SSB are from She *et al.*<sup>52</sup>

3). In contrast, evaporation was found to induce Sn isotope fractionation of up to 0.22‰ for the non-spiked NIST 3161a solution (measured by the SSB method), which highlighted the necessity of application of double spike for Sn isotope analysis of geological samples. The pure spiked NIST 3161a solutions, as well as synthetic solutions of the spiked NIST 3161a doped with matrix elements equivalent to granite, were also processed. The measured  $\delta^{122/118}\text{Sn}_{3161a}$  values of these solutions are identical to the original NIST 3161a (Table 3), validating the accuracy of chemical and mass spectrometry methods.

We also treated GSP-2 and BHVO-2 with the standard (default) one-stage TRU column procedure and the extended two-stage column (TRU + AG1-X8) procedure. The two-stage

column treatment for GSP-2 and BHVO-2 yielded the  $\delta^{122/118}\text{Sn}_{3161a}$  of  $0.209 \pm 0.011\text{‰}$  and  $0.346 \pm 0.035\text{‰}$ , which are indistinguishable from their respective average compositions measured from the default one-stage TRU column procedure. This indicates that one TRU column chemistry is sufficient for processing the geological samples in our study. In addition, multiple total procedural replicates with independent digestion, column chemistry, and isotopic measurements were performed for geological reference materials to assess the intermediate precision of the analytical method. The Sn isotope compositions of reference materials are displayed in Table 4. The measured Sn isotope data of repeated measurements at different times, independent digestions, and different column

Table 4  $\delta^{122/118}\text{Sn}_{3161a}$  values for different geological reference materials

| Sample                                       |                  | GSP-2        |                             |       | BCR-2        |                             |       | AGV-2        |                             |       | BHVO-2       |                             |       |
|--|------------------|--------------|-----------------------------|-------|--------------|-----------------------------|-------|--------------|-----------------------------|-------|--------------|-----------------------------|-------|
| Digestion date                               | Measurement date | Batch number | $\delta^{122/118}\text{Sn}$ | 2sd   |
| 2022/5/27                                    | 2022/6/22        | 2507         | 0.213                       | 0.033 | 1748         | 0.315                       | 0.035 | 531          | 0.291                       | 0.016 | 1743         | 0.357                       | 0.031 |
|  |                  |              | 0.226                       | 0.012 |              | 0.291                       | 0.022 |              |                             |       |              |                             |       |
|  |                  | 608          | 0.226                       | 0.012 | 362          | 0.331                       | 0.011 | 227          | 0.299                       | 0.043 | 3191         | 0.339                       | 0.035 |
|  |                  |              |                             |       |              |                             |       |              |                             |       |              | 0.336                       | 0.104 |
|  |                  | 2507         | 0.242                       | 0.036 | 1748         | 0.316                       | 0.042 | 531          | 0.28                        | 0.01  | 1743         | 0.357                       | 0.031 |
|  |                  |              |                             |       |              | 0.299                       | 0.025 |              |                             |       |              |                             |       |
|  |                  |              |                             |       |              | 0.33                        | 0.035 |              |                             |       |              |                             |       |
|  |                  | 608          | 0.229                       | 0.034 | 362          | 0.33                        | 0.037 | 227          | 0.284                       | 0.065 | 3191         | 0.349                       | 0.064 |
|  |                  |              | 0.227                       | 0.035 |              |                             |       |              |                             |       |              |                             |       |
| 2022/6/1                                     | 2022/6/22        | 2507         | 0.217                       | 0.069 |              |                             |       |              |                             |       | 1743         | 0.339                       | 0.016 |
| 2022/6/20                                    | 2022/7/4         | 608          | 0.209                       | 0.011 | 362          | 0.285                       | 0.014 | 227          |                             |       | 3191         | 0.346                       | 0.035 |
|  |                  | 608          | 0.199                       | 0.023 | 362          | 0.312                       | 0.039 | 227          | 0.305                       | 0.038 | 3191         | 0.367                       | 0.037 |
| 2022/7/7                                     | 2022/7/17        | 608          | 0.237                       | 0.032 |              |                             |       |              |                             |       |              |                             |       |
| 2022/7/19                                    | 2022/8/17        | 608          | 0.209                       | 0.053 |              |                             |       |              |                             |       |              |                             |       |
| 2022/8/15                                    | 2022/9/7         | 2507         | 0.246                       | 0.05  |              |                             |       |              |                             |       |              |                             |       |
| Average                                      |                  |              | 0.223                       |       |              | 0.312                       |       |              | 0.292                       |       |              | 0.349                       |       |
| 2sd  |                  |              | 0.029                       |       |              | 0.035                       |       |              | 0.021                       |       |              | 0.021                       |       |
| N  |                  |              | 12                          |       |              | 9                           |       |              | 5                           |       |              | 8                           |       |
| (Wang <i>et al.</i> , 2022) <sup>41</sup>    |                  |              | 0.24 ±                      |       |              |                             |       |              | 0.26 ±                      |       |              | 0.38 ±                      |       |
|  |                  |              | 0.12                        |       |              |                             |       |              | 0.06                        |       |              | 0.14                        |       |
| (Wang <i>et al.</i> , 20217) <sup>44</sup>   |                  |              |                             |       |              |                             |       |              |                             |       |              | 0.135 ±                     |       |
|  |                  |              |                             |       |              |                             |       |              |                             |       |              | 0.030                       |       |
| (Creech <i>et al.</i> , 20217) <sup>42</sup> |                  |              | 0.077 ±                     |       |              | 0.301 ±                     |       |              | 0.207 ±                     |       |              |                             |       |
|  |                  |              | 0.022                       |       |              | 0.065                       |       |              | 0.120                       |       |              |                             |       |

| Sample                                    |                  | GSR-1                       |       | JG-2         |                             | NOD-A-1 |              | BIR-1                       |       | RGM-1        |                             |       |              |                             |       |
|---|------------------|-----------------------------|-------|--------------|-----------------------------|---------|--------------|-----------------------------|-------|--------------|-----------------------------|-------|--------------|-----------------------------|-------|
| Digestion date                            | Measurement date | $\delta^{122/118}\text{Sn}$ | 2sd   | Batch number | $\delta^{122/118}\text{Sn}$ | 2sd     | Batch number | $\delta^{122/118}\text{Sn}$ | 2sd   | Batch number | $\delta^{122/118}\text{Sn}$ | 2sd   | Batch number | $\delta^{122/118}\text{Sn}$ | 2sd   |
| 2022/6/20                                 | 2022/7/4         | 0.215                       | 0.031 | 6-174        | 0.514                       | 0.018   | 12           | 0.343                       | 0.008 | 859          | 0.351                       | 0.036 | 53-13        | 0.206                       | 0.04  |
|   |                  | 0.251                       | 0.039 | 6-174        | 0.5                         | 0.047   | 12           | 0.315                       | 0.02  |              |                             |       |              |                             |       |
| 2022/7/7                                  | 2022/7/17        | 0.215                       | 0.017 | 6-174        | 0.488                       | 0.054   |              |                             |       | 859          | 0.334                       | 0.056 | 53-13        | 0.191                       | 0.051 |
| 2022/7/19                                 | 2022/8/17        | 0.218                       | 0.025 |              |                             |         |              |                             |       |              |                             |       |              |                             |       |
| 2022/8/15                                 | 2022/9/7         |                             |       |              |                             |         |              |                             |       |              |                             |       |              |                             |       |
| 2022/9/10                                 | 2022/9/24        | 0.248                       | 0.036 |              |                             |         |              |                             |       |              |                             |       |              |                             |       |
| Average                                   |                  | 0.229                       |       |              | 0.501                       |         |              | 0.329                       |       |              | 0.343                       |       |              | 0.199                       |       |
| 2sd                                       |                  | 0.037                       |       |              | 0.026                       |         |              | 0.04                        |       |              | 0.024                       |       |              | 0.021                       |       |
| N   |                  | 5                           |       |              | 3                           |         |              | 2                           |       |              | 2                           |       |              | 2                           |       |
| (Wang <i>et al.</i> , 2022) <sup>41</sup> |                  |                             |       |              | 0.44 ±                      |         |              | 0.28 ±                      |       |              |                             |       |              |                             |       |
|   |                  |                             |       |              | 0.10                        |         |              | 0.04                        |       |              |                             |       |              |                             |       |

chemistry over four months were consistent, attesting to the robustness of our double-spike Sn isotope analytical method. The repeated measurements of NOD-A-1 yield the largest 2SD error of  $\pm 0.040\%$  among replicates of reference materials, which is within the largest error ( $\pm 0.069\%$ ) determined for the individual GSP-2. Therefore, we conservatively estimate that the intermediate precision in our method was better than  $\pm 0.069\%$  on  $\delta^{122/118}\text{Sn}$ .

#### 4.6. Sn content and isotopic composition of geological reference materials

Previous studies have determined the Sn concentrations of geological reference materials with various methods, including isotope dilution (ID) ICP-MS, ID-TIMS, LA-ICP-MS, and standard addition ICP-QMS,<sup>41,89–92</sup> however, the reported data are quite variable. The isotope dilution method is a powerful method to determine elemental concentration data precisely for geological materials. In this study, the double spike method could provide the most precise Sn concentration data because the analytical error would mainly arise from sample weighing and pipetting of spike solution. The Sn mass fractions of these geological reference materials are reported in Table S3.<sup>†</sup> The error for most of the Sn concentration data was within 0.05%, except for AGV-2 that has an error of 9%, which could be due to sample heterogeneity. The measured Sn contents are consistent with previous determinations for the reference materials analyzed in this study. Specifically, the Sn content measured for BHVO-2 ( $1.83 \pm 0.05 \mu\text{g g}^{-1}$ ,  $N = 7$ ) is in agreement with the literature data of 1.70 to 2.3  $\mu\text{g g}^{-1}$ .<sup>41,42,89,93,94</sup> The Sn contents of other geological reference materials determined in this study (Fig. 10) are also in good agreement with the data from the literature.<sup>8,41,42,89–91,93</sup>

To date, only three other laboratories have established the method for high-precision stable Sn isotope measurements on geological reference materials.<sup>41,42,44</sup> However, there had been some inconsistency in the reported Sn isotope compositions for

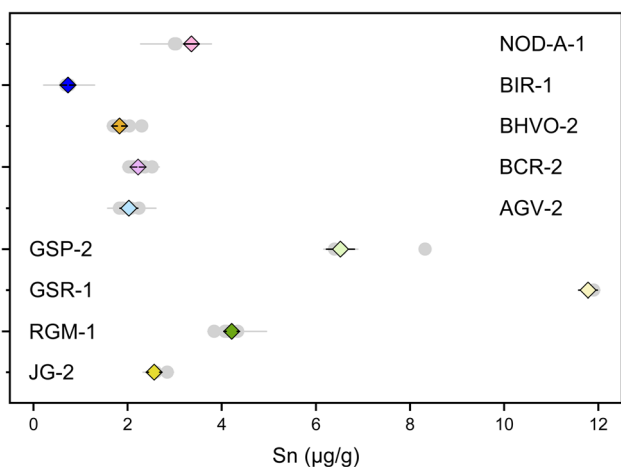


Fig. 10 Sn contents of geological reference materials. The grey dots are data from the literature. The diamonds are data from this study. All uncertainties on individual data points reflect the 2SD of the samples.

the geological reference materials, especially for BHVO-2.<sup>41</sup> This could be due to Sn isotopic heterogeneity between different batches of reference materials or insufficient replicates.<sup>41</sup> In this study, we used the different batches of BHVO-2 (#1743 and #3191), GSP-2 (#0527 and #0608), AGV-2 (#531 and #227), and BCR-2 (#1748 and #0362), performing independent digestion and measurements to test if there is any significant Sn isotope

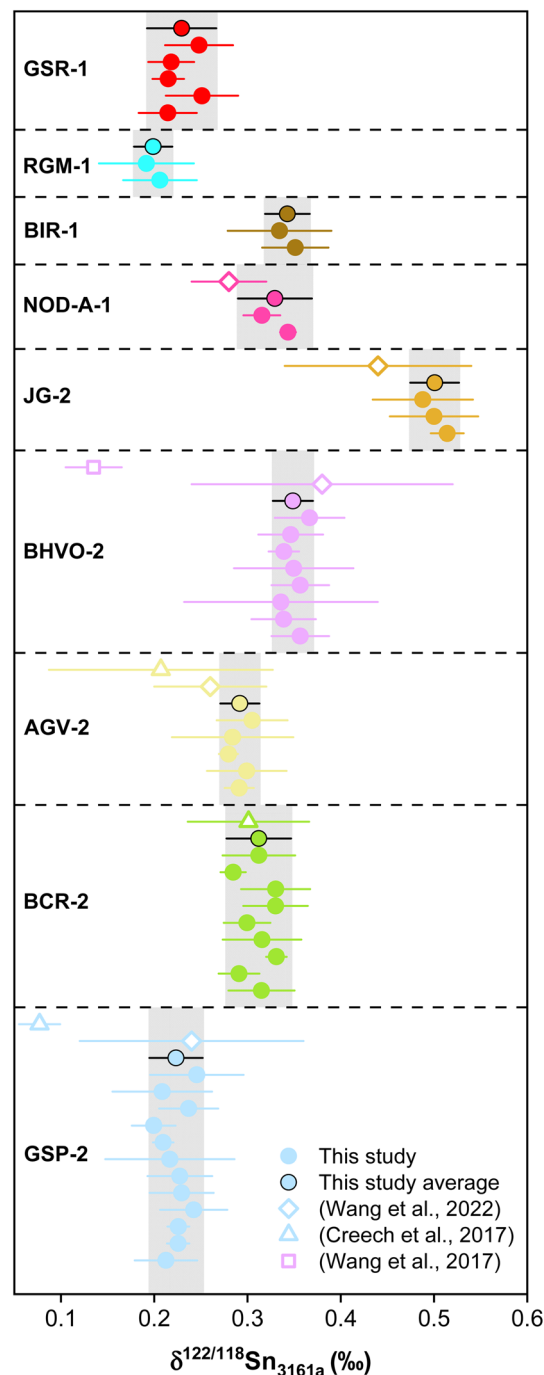


Fig. 11 The  $\delta^{122/118}\text{Sn}_{3161a}$  compositions of reference materials with various rock types and Sn mass fractions. The solid points are data from this study, while the open symbols represent the literature data (Creech *et al.*, 2017;<sup>42</sup> Wang *et al.*, 2017;<sup>44</sup> Wang *et al.*, 2022).<sup>41</sup> Errors in data reflect two standard deviations (2SD).

difference between different batches (aliquots) of geological reference materials (Table 4). The repeated digestions and measurements of BHVO-2 yielded a  $\delta^{122/118}\text{Sn}_{3161a}$  of  $0.349 \pm 0.021\%$  ( $N = 8$ ), which is in agreement with the result of Wang *et al.* (2022),<sup>41</sup> ( $\delta^{122/118}\text{Sn}_{3161a}$  of  $0.38 \pm 0.14\%$ ) but slightly higher than that of Wang *et al.* (2017),<sup>44</sup> (Fig. 11). The  $\delta^{122/118}\text{Sn}_{3161a}$  value for GSP-2, AGV-2, JG-2, and NOD-A-1 are  $0.223 \pm 0.029\%$  ( $N = 12$ ),  $0.292 \pm 0.021\%$  ( $N = 5$ ),  $0.501 \pm 0.026\%$  ( $N = 3$ ), and  $0.329 \pm 0.040\%$  ( $N = 2$ ), respectively, which are also consistent with the data of Wang *et al.* (2022).<sup>41</sup> The BCR-2 has  $\delta^{122/118}\text{Sn}_{3161a}$  of  $0.312 \pm 0.035\%$  ( $N = 12$ ). We found that the Sn isotope compositions of BCR-2 and AGV-2 from Creech *et al.*<sup>42</sup> are in agreement with this study, whereas the  $\delta^{122/118}\text{Sn}_{3161a}$  of GSP-2 is slightly lower in their result, assuming that BHVO-2 from both studies has an identical composition. The consistency of our replicate digestions and measurements for geological reference materials of different batches confirms the representativeness and reliability of our data. Furthermore, our results support the consistency of the Sn isotope composition of NIST 3161a with different batch numbers (#140917 *versus* #070330). We propose that future studies could report Sn isotope data with reference to NIST 3161a and Sn isotope data for the above USGS rock standards for data validation.

In addition to the geological reference materials reported for Sn isotopes in previous studies, we also measured the Sn isotope composition of three new geological reference materials that had not been reported before. The rock standards of BIR-1, RGM-1, and GSR-1 yield the  $\delta^{122/118}\text{Sn}_{3161a}$  values of  $0.343 \pm 0.024\%$  ( $N = 2$ ),  $0.199 \pm 0.021\%$  ( $N = 2$ ) and  $0.229 \pm 0.037\%$  ( $N = 5$ ). Overall, the results reveal large Sn isotope variations for the magmatic rocks, suggesting the potential of Sn isotopes for tracing magmatic-hydrothermal processes. Granite is the most abundant felsic intrusive rock on the upper continental crust. The  $\delta^{122/118}\text{Sn}_{3161a}$  variation for the granitic reference materials is up to  $0.278\%$ , which signifies the Sn isotopic heterogeneity for the upper continental crust.

## 5. Conclusion

This study reports a high-precision Sn isotope measurement method with  $^{117}\text{Sn}$ – $^{122}\text{Sn}$  double spike MC-ICP-MS. The factors affecting the accuracy and repeatability of Sn isotope measurements are systematically evaluated. The results show that matrix elements do not affect Sn isotope measurements with the mass ratios of  $[X]/\text{Sn}$  ( $\text{ng g}^{-1}/\text{ng g}^{-1}$ ) lower than 0.5, except for Cd. Further tests demonstrate that the acid mismatch induces no resolvable Sn isotopic offset. At the same time,  $\delta^{122/118}\text{Sn}$  can be affected by the Sn concentration difference between the sample and bracketing standard, and a Sn concentration matching of better than  $\pm 20\%$  is needed to ensure accurate and precise Sn isotopic measurements. Based on repeated measurements, the long-term intermediate precision of our method is better than  $\pm 0.069\%$ . We provide precise Sn contents and isotopic compositions for nine geological reference materials, reproducible and consistent with the previous study. Furthermore, the overall variation of reference materials is  $0.30\%$  in  $\delta^{122/118}\text{Sn}$ , indicating that Sn isotopes are

fractionated significantly during various Earth's processes, including high-temperature magmatic processes.

## Author contributions

Jia-Xin She, data curation, formal analysis, visualization, writing—original draft; Weiqiang Li, supervision, conceptualization, funding acquisition, formal analysis, writing—review and editing; Shichao An, methodology, formal analysis; Yuanfeng Cai, supervision, resources, validation.

## Conflicts of interest

There are no conflicts of interest to declare.

## Acknowledgements

We thank Ruiyu Yang and John Creech for discussions on double spike. SJX is supported by a grant from the China Scholarship Council (File No. 202006190253) and program B for the Outstanding PhD candidate of Nanjing University (File No. 202201B047). This study is supported by the Fundamental Research Funds for the Central Universities (14380165, 14380126, 14380141 to WL).

## References

- 1 W. Yi, A. N. Halliday, D.-C. Lee and J. N. Christensen, *Geochim. Cosmochim. Acta*, 1995, **59**, 5081–5090.
- 2 G. Witt-Eickschen, H. Palme, H. S. C. O'Neill and C. M. Allen, *Geochim. Cosmochim. Acta*, 2009, **73**, 1755–1778.
- 3 C. A. Heinrich, *Econ. Geol. Bull. Soc. Econ. Geol.*, 1990, **85**, 457–481.
- 4 F.-Z. Teng, N. Dauphas, J. M. Watkins and De Gruyter, *Non-Traditional Stable Isotopes: Retrospective and Prospective*, Berlin, Boston, 2017, pp. 1–26.
- 5 N. Badullovich, F. Moynier, J. Creech, F. Z. Teng and P. A. Sossi, *Geochem. Perspect. Lett.*, 2017, **5**, 24–28.
- 6 M. Roskosz, Q. Amet, C. Fitoussi, N. Dauphas, B. Bourdon, L. Tissandier, M. Y. Hu, A. Said, A. Alatas and E. E. Alp, *Geochim. Cosmochim. Acta*, 2020, **268**, 42–55.
- 7 T. Wang, J.-X. She, K. Yin, K. Wang, Y. Zhang, X. Lu, X. Liu and W. Li, *Geochim. Cosmochim. Acta*, 2021, **300**, 25–43.
- 8 X. Wang, Q. Amet, C. Fitoussi and B. Bourdon, *Geochim. Cosmochim. Acta*, 2018, **228**, 320–335.
- 9 J. Yao, R. Mathur, W. Powell, B. Lehmann, F. Tornos, M. Wilson and J. Ruiz, *Am. Mineral.*, 2018, **103**, 1591–1598.
- 10 I. M. Chou, R. Wang and J. Fang, *Geochem. Perspect. Lett.*, 2021, 1–5, DOI: [10.7185/geochemlet.2135](https://doi.org/10.7185/geochemlet.2135).
- 11 C. Schmidt, *Geochim. Cosmochim. Acta*, 2018, **220**, 499–511.
- 12 D. Duce, S. Salah, L. Wang and N. Maes, *Appl. Geochem.*, 2020, **123**, 104775.
- 13 Y. Cheng, C. Spandler, A. Kemp, J. Mao, B. Rusk, Y. Hu and K. Blake, *Am. Mineral.*, 2019, **104**, 118–129.
- 14 Q. Qu, G. Liu, R. Sun and Y. Kang, *Environ. Geochem. Health*, 2016, **38**, 1–23.

- 15 R. C. Wang, L. Xie, J. Chen, A. Yu, L. Wang, J. Lu and J. Zhu, *J. Asian Earth Sci.*, 2013, **74**, 361–372.
- 16 B. Lehmann, *Lithos*, 2021, 402–403.
- 17 K. J. Jackson and H. C. Helgeson, *Geochim. Cosmochim. Acta*, 1985, **49**, 1–22.
- 18 V. J. Wall and J. R. Taylor, *Econ. Geol.*, 1993, **88**, 437–460.
- 19 B. E. Kunz, C. J. Warren, F. E. Jenner, N. B. W. Harris and T. W. Argles, *Geology*, 2022, **50**(11), 1219–1223.
- 20 P. Carr, M. D. Norman, V. C. Bennett and P. L. Blevin, *Econ. Geol.*, 2020, **116**, 147–167.
- 21 M. Harlaux, K. Kouzmanov, S. Gialli, O. Laurent, A. Rielli, A. Dini, A. Chauvet, A. Menzies, M. Kalinaj and L. Fontboté, *Econ. Geol.*, 2020, **115**, 1665–1697.
- 22 R. L. Romer and U. Kroner, *Gondwana Res.*, 2016, **31**, 60–95.
- 23 S. s. Sun and W. F. McDonough, *Geol. Soc. Spec. Publ.*, 1989, **42**, 313–345.
- 24 R. L. Rudnick and S. Gao, in *Treatise on Geochemistry*, ed. H. D. Holland and K. K. Turekian, Pergamon, Oxford, 2003, pp. 1–64, DOI: [10.1016/B0-08-043751-6/03016-4](https://doi.org/10.1016/B0-08-043751-6/03016-4).
- 25 N. J. McNaughton and K. J. R. Rosman, *Geochim. Cosmochim. Acta*, 1991, **55**, 499–504.
- 26 R. D. Loss, K. J. R. Rosman and J. R. Delaeter, *Geochim. Cosmochim. Acta*, 1990, **54**, 3525–3536.
- 27 D. D. Clayton, W. A. Fowler, T. E. Hull and B. A. Zimmerman, *Ann. Phys.*, 1961, **12**, 331–408.
- 28 J. R. De Laeter and P. M. Jeffery, *J. Geophys. Res.*, 1965, **70**, 2895–2903.
- 29 J. B. Creech, F. Moynier and C. Koeberl, *Chem. Geol.*, 2019, **528**, 119279.
- 30 Q. Qu, G. Liu, M. Henry, D. Point, J. Chmeleff, R. Sun, J. E. Sonke and J. Chen, *Appl. Geochem.*, 2020, **119**, 104641.
- 31 X. Wang, C. Fitoussi, B. Bourdon, B. Fegley and S. Charnoz, *Nat. Geosci.*, 2019, **12**, 707–711.
- 32 M. Haustein, C. Gillis and E. Pernicka, *Archaeometry*, 2010, **52**, 816–832.
- 33 E. Yamazaki, S. Nakai, Y. Sahoo, T. Yokoyama, H. Mifune, T. Saito, J. Chen, N. Takagi, N. Hokanishi and A. Yasuda, *J. Archaeol. Sci.*, 2014, **52**, 458–467.
- 34 D. Berger, G. Brüggemann and E. J. A. Pernicka, *Archaeol. Anthropol. Sci.*, 2019, **11**, 293–319.
- 35 A. Mason, W. Powell, H. A. Bankoff, R. Mathur, M. Price, A. Bulatović and V. Filipović, *J. Archaeol. Sci.*, 2020, **122**, 105181.
- 36 C. Devillers, T. Lecomte and R. Hagemann, *Int. J. Mass Spectrom. Ion Phys.*, 1983, **50**, 205–217.
- 37 K. J. R. Rosman and N. J. McNaughton, *Int. J. Mass Spectrom. Ion Processes*, 1987, **75**, 91–98.
- 38 N. H. Gale, *Archaeometry*, 1997, **39**, 71–82.
- 39 R. Clayton, P. Andersson, N. H. Gale, C. Gillis and M. J. Whitehouse, *J. Anal. At. Spectrom.*, 2002, **17**, 1248–1256.
- 40 F. Moynier, T. Fujii and P. Telouk, *Anal. Chim. Acta*, 2009, **632**, 234–239.
- 41 Z. Y. Wang, Z. Y. Luo, L. Zhang, J. J. Liu and J. Li, *Geostand. Geoanal. Res.*, 2022, **46**, 547–561.
- 42 J. B. Creech, F. Moynier and N. Badullovich, *Chem. Geol.*, 2017, **457**, 61–67.
- 43 M. Friebe, E. R. Toth, M. A. Fehr and M. Schönbacher, *J. Anal. At. Spectrom.*, 2020, **35**, 273–292.
- 44 X. Wang, C. Fitoussi, B. Bourdon and Q. Amet, *J. Anal. At. Spectrom.*, 2017, **32**, 1009–1019.
- 45 Z.-H. Zhou, J.-W. Mao, J.-Q. Zhao, X. Gao, S. Weyer, I. Horn, F. Holtz, P. A. Sossi and D.-C. Wang, *Am. Mineral.*, 2022, **107**, 2111–2127.
- 46 P. Liu, J. Mao, B. Lehmann, S. Weyer, I. Horn, R. Mathur, F. Wang and Z. Zhou, *Am. Mineral.*, 2021, **106**, 1980–1986.
- 47 R. Mathur, W. Powell, A. Mason, L. Godfrey, J. Yao and M. E. Baker, *Geostand. Geoanal. Res.*, 2017, **41**, 701–707.
- 48 E. Balliana, M. Aramendía, M. Resano, C. Barbante and F. J. A. Vanhaecke, *Anal. Bioanal. Chem.*, 2013, **405**, 2973–2986.
- 49 A. H. Mason, W. G. Powell, H. A. Bankoff, R. Mathur, A. Bulatović, V. Filipović and J. Ruiz, *J. Archaeol. Sci.*, 2016, **69**, 110–117.
- 50 C. N. Marechal, P. Telouk and F. Albarede, *Chem. Geol.*, 1999, **156**, 251–273.
- 51 F. Albarède and B. Beard, *Rev. Mineral. Geochem.*, 2004, **55**, 113–152.
- 52 J.-X. She, T. Wang, H. Liang, M. N. Muhtar, W. Li and X. Liu, *Geochim. Cosmochim. Acta*, 2020, **269**, 184–202.
- 53 D. Wang, R. Mathur, W. Powell, L. Godfrey and Y. Zheng, *Geochim. Cosmochim. Acta*, 2019, **250**, 209–218.
- 54 D. Berger, E. Figueiredo, G. Brüggemann and E. Pernicka, *J. Archaeol. Sci.*, 2018, **92**, 73–86.
- 55 J. F. Rudge, B. C. Reynolds and B. Bourdon, *Chem. Geol.*, 2009, **265**, 420–431.
- 56 M. Klaver and C. D. Coath, *Geostand. Geoanal. Res.*, 2018, **43**, 5–22.
- 57 B. Andris and J. Beňa, *J. Radioanal. Nucl. Chem.*, 2016, **308**, 781–788.
- 58 T. N. der Walt and P. P. Coetzee, *Fresenius' J. Anal. Chem.*, 1996, **356**, 425–429.
- 59 E. P. Horwitz, R. Chiarizia, M. L. Dietz, H. Diamond and D. M. Nelson, *Anal. Chim. Acta*, 1993, **281**, 361–372.
- 60 H. L. Zhu, Z. F. Zhang, G. Q. Wang, Y. F. Liu, F. Liu, X. Li and W. D. Sun, *Geostand. Geoanal. Res.*, 2016, **40**, 185–194.
- 61 A. D. Anbar, J. E. Roe, J. Barling and K. H. Nealson, *Science*, 2000, **288**, 126–128.
- 62 L. A. Machlan and J. W. Gramlich, *Anal. Chem.*, 1988, **60**, 37–39.
- 63 C. Maréchal and F. Albarède, *Geochim. Cosmochim. Acta*, 2002, **66**, 1499–1509.
- 64 Y. Tachibana, Y. Yamazaki, M. Nomura and T. Suzuki, *J. Radioanal. Nucl. Chem.*, 2015, **303**, 1429–1434.
- 65 D. Nickel, M. Haustein, T. Lampke and E. Pernicka, *Archaeometry*, 2012, **54**, 167–174.
- 66 E. Yamazaki, S. i. Nakai, T. Yokoyama, S. Ishihara and H. Tang, *Geochem. J.*, 2013, **47**, 21–35.
- 67 K. Shuai, W. Li and H. Hui, *Anal. Chem.*, 2020, **92**, 4820–4828.
- 68 X. Wang and T. M. Johnson, *Anal. Chem.*, 2021, **93**, 7449–7455.
- 69 T. M. Johnson, M. J. Herbel, T. D. Bullen and P. T. Zawislanski, *Geochim. Cosmochim. Acta*, 1999, **63**, 2775–2783.

- 70 C. M. Johnson and B. L. Beard, *Int. J. Mass Spectrom.*, 1999, **193**, 87–99.
- 71 C. Siebert, T. F. Nägler and J. D. Kramers, *Geochem., Geophys., Geosyst.*, 2001, **2**, 2000GC000124.
- 72 H.-G. Zhu, J.-M. Zhu, D. Tan, X. Lin, K. Lu and W. Yang, *J. Anal. At. Spectrom.*, 2022, **37**, 1063–1075.
- 73 D. Tan, J.-M. Zhu, X. Wang, G. Han, Z. Lu and W. Xu, *J. Anal. At. Spectrom.*, 2020, **35**, 713–727.
- 74 E. C. Inglis, J. B. Creech, Z. Deng and F. Moynier, *Chem. Geol.*, 2018, **493**, 544–552.
- 75 L.-L. Tian, Y.-Z. Gong, W. Wei, J.-T. Kang, H.-M. Yu and F. Huang, *J. Anal. At. Spectrom.*, 2020, **35**, 1566–1573.
- 76 L.-L. Tian, Z. Zeng, X.-Y. Nan, H.-M. Yu and F. Huang, *J. Anal. At. Spectrom.*, 2019, **34**, 1459–1467.
- 77 K. Moeller, R. Schoenberg, R.-B. Pedersen, D. Weiss and S. Dong, *Geostand. Geoanal. Res.*, 2012, **36**, 177–199.
- 78 F. Moynier, Y. Hu, K. Wang, Y. Zhao, Y. Gérard, Z. Deng, J. Moureau, W. Li, J. I. Simon and F.-Z. Teng, *Chem. Geol.*, 2021, **571**, 120144.
- 79 D. Malinovsky, A. Stenberg, I. Rodushkin, H. Andren, J. Ingri, B. Öhlander and D. C. Baxter, *J. Anal. At. Spectrom.*, 2003, **18**, 687–695.
- 80 M. S. Liu, Q. Zhang, Y. Zhang, Z. Zhang, F. Huang and H. M. Yu, *Geostand. Geoanal. Res.*, 2019, **44**, 169–182.
- 81 X. Nan, F. Wu, Z. Zhang, Z. Hou, F. Huang and H. Yu, *J. Anal. At. Spectrom.*, 2015, **30**, 2307–2315.
- 82 M.-L. Pons, M.-A. Millet, G. N. Nowell, S. Misra and H. M. Williams, *J. Anal. At. Spectrom.*, 2020, **35**, 320–330.
- 83 S. An, X. Luo and W. Li, *Rapid Commun. Mass Spectrom.*, 2022, **36**, e9289.
- 84 M. A. Fehr, M. Rehkämper and A. N. Halliday, *Int. J. Mass Spectrom.*, 2004, **232**, 83–94.
- 85 V. Yilmaz, L. Rose, Z. Arslan and M. D. Little, *J. Anal. At. Spectrom.*, 2012, **27**, 1895–1902.
- 86 X. Liu, L. Chen, H. Peng, G. Wang, N. S. Belshaw, H. Zheng, S. Hu and Z. Zhu, *Anal. Chim. Acta*, 2022, **1215**, 339980.
- 87 G. Brueggemann, D. Berger and E. Pernicka, *Geostand. Geoanal. Res.*, 2017, **41**, 437–448.
- 88 M. Schulze, M. Ziegerick, I. Horn, S. Weyer and C. Vogt, *Spectrochim. Acta, Part B*, 2017, **130**, 26–34.
- 89 N. Braukmüller, F. Wombacher, A. Bragagni and C. Münker, *Geostand. Geoanal. Res.*, 2020, **44**, 733–752.
- 90 A. J. B. Cotta and J. Enzweiler, *Geostand. Geoanal. Res.*, 2013, **37**, 35–50.
- 91 K. P. Jochum, U. Weis, B. Schwager, B. Stoll, S. A. Wilson, G. H. Haug, M. O. Andreae and J. Enzweiler, *Geostand. Geoanal. Res.*, 2016, **40**, 333–350.
- 92 Y. Lu, A. Makishima and E. Nakamura, *Chem. Geol.*, 2007, **236**, 13–26.
- 93 M. Kirchenbaur, A. Heuser, A. Bragagni and F. Wombacher, *Geostand. Geoanal. Res.*, 2018, **42**, 361–377.
- 94 D. Weis, B. Kieffer, C. Maerschalk, W. Pretorius and J. Barling, *Geochem., Geophys., Geosyst.*, 2005, **6**(2), 2004GC000852.